Journal of Solid State Chemistry **161,** 45–56 (2001)
doi:10.1006/jssc.2001.9265, available online at http://www.idealibrary.com on IDEAL®

Phase Relations in the System Fe_2O_3–Cr_2O_3–TiO_2 between 1000 and 1300°C and the Stability of $(Cr,Fe)_2Ti_{n-2}O_{2n-1}$ Crystallographic Shear Structure Compounds

Mark I. Pownceby, Michael J. Fisher-White, and Varghese Swamy

CSIRO Minerals, Box 312, Clayton South, Victoria 3169 Australia

Received February 9, 2001; in revised form May 24, 2001; accepted June 7, 2001; published online August 24, 2001

Phase relations and the stability of crystallographic shear (*CS*) structure compounds $(Cr,Fe)_2Ti_{n-2}O_{2n-1}$ in the system Fe_2O_3–Cr_2O_3–TiO_2 were investigated between 1000 and 1300°C. The ternary comprises five major solid solution series. These are as follows: an M_2O_3 series; an M_3O_5 series made up of two separate solid solution series—the first an orthorhombic pseudobrookite M_3O_5 solid solution and the second a monoclinic M_3O_5 series based on the V_3O_5 structure type; an M_4O_7 series; and an M_5O_9 series. These latter three series represent lower homologues ($n = 3$, 4, and 5) of the $(Cr,Fe)_2Ti_{n-2}O_{2n-1}$ *CS* compound series. Between adjacent M_3O_5 and M_4O_7 and M_4O_7 and M_5O_9 solid solutions, ordered intergrowths may occur. The stability and compositional limits of the solid solution series and intergrowth phases are dependent upon the temperature and Fe:Cr ratio. At high-TiO_2 contents, assemblages may contain either members of the Andersson phase series $Cr_2Ti_{n-2}O_{2n-1}$, a continuous *CS* structure series extending into the ternary, or a rutile-based solid solution. A comparison of results from this study with previously published phase relations has led to a revised version of the Fe_2O_3–Cr_2O_3–TiO_2 phase diagram.

Key Words: **phase relations; Fe_2O_3–Cr_2O_3–TiO_2 system; crystallographic shear structure compounds.**

INTRODUCTION

Well-established phase diagrams are available for the systems Fe_2O_3–Cr_2O_3 (1) and Fe_2O_3–TiO_2 (2–4), two of the limiting binary systems within the Fe_2O_3–Cr_2O_3–TiO_2 ternary. Cr_2O_3 and Fe_2O_3 exhibit complete solid solution between the end members at 1200°C, while for Fe_2O_3–TiO_2, in addition to the end members hematite and rutile, the binary join also includes pseudobrookite above 585°C (5) and may contain metastable pseudorutile, $Fe_2Ti_3O_9$ (6).

The third system Cr_2O_3–TiO_2 is more complex due to the presence at the TiO_2-rich end of the binary of (a) a rutile structure-defect solid solution and (b) two series of crystallographic shear (*CS*) structure compounds (7,8). The first *CS* region was studied by Andersson *et al.* (9) who revealed the existence of a number of discrete compounds of the general form $Cr_2Ti_{n-2}O_{2n-1}$ where $n = 6, 7, 8$, and 9. These compounds, referred to as Andersson phases (AP), are isomorphous with members of the homologous series Ti_nO_{2n-1} (10) and V_nO_{2n-1} (11). In addition to the AP series (but occurring at a higher TiO_2 content), there is a continuous series of well-ordered *CS* structure phases. In these phases, the slabs of rutile structure (the normal spacing between recurrent shear planes) remain constant, but the orientation of the shear planes pivots round progressively from $(121)_r$ to $(132)_r$ as the anion:cation ratio is changed (7, 8).

For the lower homologues ($n = 3, 4$, and 5) within the $Cr_2Ti_{n-2}O_{2n-1}$ series, Åsbrink *et al.* (12) demonstrated that the composition Cr_2TiO_5 ($n = 3$) can be stabilized in a form isomorphous with V_3O_5 by the addition of Fe_2TiO_5 or Al_2TiO_5. $Cr_2Ti_2O_7$ ($n = 4$) was first identified as a discrete compound, not part of the AP series, by Hamélin (13). Studies by Flörke and Lee (14) have indicated that it is non stoichiometric below 1500°C and has an apparent range of homogeneity. Sōmiya *et al.* (15) report $Cr_2Ti_3O_9$ ($n = 5$) as being stable between 1250 and 1300°C. Above $\sim$ 1300°C, $Cr_2Ti_3O_9$ breaks down to Andersson phases ($n \geq 6$). The low temperature stability is unknown.

To further examine the stabilizing effect of Fe^{3+} on compounds such as Cr_2TiO_5 as observed by Åsbrink *et al.* (12), subsolidus phase relations in the system Fe_2O_3–Cr_2O_3–TiO_2 were determined at 1300°C by Kwestroo and Roos (16). Their study demonstrated the existence of a series of monoclinic compounds of the general formula $Cr_2Ti_{n-2}O_{2n-1}$ ($n = 6, 7, 8$, and 9) and three distinct iron–chromium titanate solid solution series. In one solid solution, about two-thirds of the Cr^{3+} ions in $Cr_2Ti_2O_7$ could be replaced by Fe^{3+} without any change in the structure. The second solid solution is a pseudobrookite solid solution extending from Fe_2TiO_5 to $(Fe_{0.85}Cr_{0.15})_2TiO_5$. The third solid solution, with the V_3O_5 structure, ranged in composition from $(Fe_{0.10}Cr_{0.90})_2TiO_5$ to $(Fe_{0.45}Cr_{0.55})_2TiO_5$. This V_3O_5

0022-4596/01 $35.00

phase was analogous to the compound found in the neighborhood of Cr_2TiO_5 by Hamélin (13) and also with the phase found by Åsbrink *et al.* (12).

In a series of papers, Grey and Reid (17) and Grey and Mumme (18) demonstrated that lower homologues of the $Cr_2Ti_{n-2}O_{2n-1}$ series (i.e., $n = 3, 4$, and 5) could also be stabilized by the addition of Fe^{3+}. The first member of the series, $n = 3$, was equivalent to the V_3O_5 structure solid solution series determined by Kwestroo and Roos (16), while the remaining two members ($n = 4$ and 5) may be described as ordered intergrowths of the V_3O_5 and α-PbO_2 structural types. Above 1450°C, the powder patterns of the compounds changed to that intermediate between M_3O_5 and M_4O_7 and are represented by the general formula $(M_3O_5)_n(M_4O_7)_m$. The $(Cr,Fe)_2Ti_2O_7$ compounds were stable to 1500°C and the temperature of the formation of a single phase of the form M_4O_7 (M = Fe or Cr) increased as the Cr contents increased. Pure $Cr_2Ti_2O_7$ only formed above 1550°C. Below this temperature, $Cr_2Ti_2O_7$ formed a rutile-based AP plus new phases whose powder patterns were intermediate between those of M_4O_7 and M_5O_9 structures based on the α-PbO_2 type.

To date there has been no attempt to systematically examine the stability and compositional ranges of these phases at lower temperatures. The present study of the Fe_2O_3–Cr_2O_3–TiO_2 system between 1000 and 1200°C in air was therefore undertaken to (1) determine the location of phase boundaries at low temperatures (i.e., below 1300°C), (2) obtain the compositions and ranges of coexisting members of solid solution series, and (3) further investigate the development of crystallographic shear structure compounds and intergrowths in chromium–iron titanates at low temperatures. Based on the results from the 1000–1200°C experiments, a re-examination of the phase relations in the Fe_2O_3–Cr_2O_3–TiO_2 system at 1300°C was also conducted.

EXPERIMENTAL

Sample Preparation

Experiments were based on synthetic samples made from mixtures of calculated amounts of the component oxides Fe_2O_3 (99.99%), Cr_2O_3 (99.99%), and TiO_2 (anatase form, 99.99%). Accurately calculated and weighed amounts of the dehydrated starting materials were ground thoroughly together in an agate mortar under acetone until homogenized (usually 30–45 min) and then were dried. Up to 65 compositions were prepared. Starting compositions are listed in Table 1 and plotted on the Fe_2O_3–Cr_2O_3–TiO_2 ternary in Fig. 1.

Approximately 1.3 g of each sample was pelletized using a hardened stainless steel die. Pellets were considered particularly effective for the phase equilibrium studies by ensuring rapid reaction resulting from intimate contact between oxide particles. For each composition, two separate pellets were prepared: one pellet to be crushed for powder X-ray diffraction analysis (PXRD), and the second reserved for electron microprobe (EMP) analysis. Pellets were stored under vacuum until required.

Equilibration Procedure

Pellets were placed inside small pots (6 mm OD, 4 mm ID, 10 mm tall) manufactured from calcia-stabilized zirconia (15 mol% CaO), which make good inert sample holders. The CSZ pots were contained in a platinum holder which allowed up to 25–30 separate compositions to be annealed in each experiment. Samples were then positioned carefully in the previously measured constant temperature zone of a large diameter (50 mm ID) vertical tube furnace. Annealing times were on the order of > 300 h in the 1200°C high-temperature runs, whereas a minimum of 900 h was employed for experiments at 1000°C (including at least one regrind step at each isotherm). Experiments were terminated by quenching the samples in liquid nitrogen. The temperature during each experiment was measured using a Pt–$Pt_{87}Rh_{13}$ (Type R) thermocouple positioned directly next to the sample(s). The thermocouple was calibrated against the melting point of gold. Temperatures were recorded to the nearest 0.5°C, and are probably accurate to $\pm$ 2–3°C (allowing for possible radial gradients and effects of thermal convection). Temperatures in the furnaces could be held steady to $\pm$ 2°C for weeks, if not longer, while short-term fluctuations on an hour time scale were less than $\pm$ 0.5°C.

Analytical

Diffraction studies. Phases present in the quenched samples were identified by powder X-ray diffraction (PXRD). Samples for PXRD were prepared by grinding part of each reaction pellet under acetone in a silica mortar and pestle and sedimenting a thin layer of sample onto a silicon metal zero-background plate. Measurements of diffracted intensities were obtained using a Philips 1050 XPERT goniometer with a PW1710 controller and employing Cu$K\alpha$ radiation. The diffractometer was configured with a 1°-divergent slit, 0.2-mm receiving slit, 1°-scatter slit, incident and diffracted beam Soller slits, and a diffracted-beam curved graphite monochromator. Patterns were obtained over the range 15° to 65° 2θ, with a step size of 0.02° and counting times of 4.0 s/step. Total scan times were of the order of 3 h/sample. The relatively long scan times were considered necessary, especially when close to phase boundaries, where the proportions of some phases may be at a minimum.

The triclinic $(121)_r$ continuous *CS* phases were identified from the presence and degree of separation of peaks between 28° and 29° 2θ (slightly higher angle than TiO_2) while the series of monoclinic $(Cr,Fe)_2Ti_{n-2}O_{2n-1}$ homologous

TABLE 1
Summary of Starting Compositions for Phase Equilibrium Experiments in the System Fe_2O_3–Cr_2O_3–TiO_2

Sample no.	Mole %			Cr/(Cr + Fe)	Sample no.	Mole %			Cr/(Cr + Fe)
	Fe_2O_3	Cr_2O_3	TiO_2			Fe_2O_3	Cr_2O_3	TiO_2	
1	70	10	20	0.125	34	6	9	85	0.600
2	60	20	20	0.250	35	2	46	52	0.958
3	60	10	30	0.143	36	4	46	50	0.920
4	60	5	35	0.077	37	6	46	48	0.885
5	50	10	40	0.167	38	6	20	74	0.769
6	50	5	45	0.091	39	22.5	11	66.5	0.328
7	40	20	40	0.333	40	28.5	5	66.5	0.149
8	40	10	50	0.200	41	26.3	7	66.7	0.210
9	40	5	55	0.111	42	24.3	9	66.7	0.270
10	30	20	50	0.400	43	2	23	75	0.920
11	30	10	60	0.250	44	6	34	60	0.850
12	30	5	65	0.143	45	4	36	60	0.900
13	20	40	40	0.667	46	8	46	46	0.852
14	20	20	60	0.500	47	6	24	70	0.800
15	20	10	70	0.333	48	8	29.5	62.5	0.787
16	20	5	75	0.200	49	1.5	8	90.5	0.842
17	10	30	60	0.750	50	0	13.5	86.5	1.000
18	10	20	70	0.667	51	0	28	72	1.000
19	10	10	80	0.500	52	1.5	15.5	83	0.912
20	10	5	85	0.333	53	2	96	2	0.980
21	14	5	81	0.263	54	2	21	77	0.913
22	23	3	74	0.115	55	6	29	65	0.829
23	20	6	74	0.231	56	9	36	55	0.800
24	17	9	74	0.346	57	1.5	25.5	73	0.944
25	14	12	74	0.462	58	1.5	29.5	69	0.952
26	10	16	74	0.615	59	1.5	32.5	66	0.956
27	48	7	45	0.127	60	3	3	94	0.500
28	41	14	45	0.255	61	25	1	74	0.038
29	35	20	45	0.364	62	24	2	74	0.077
30	37.5	7.5	55	0.167	63	17	2	81	0.105
31	35	10	55	0.222	64	30	0	70	0.000
32	30	15	55	0.333	65	80	0	20	0.000
33	6	15	79	0.714					

compounds ($n = 3, 4,$ and 5) and their possible ordered intergrowths were identified using the change in d-spacing for the peak between approximately 18.9° and 22° 2θ. The position of this peak showed the greatest variation according to the phase present. Peak position data were compared with observed $\sin^2\theta$ values given for these phases in the series of papers by Grey and Reid (17) and Grey *et al.* (19). Assigning peaks to various phases was not always straightforward, however, as many of the M_5O_9 and other monoclinic phase peaks encountered were broad (particularly when ordered intergrowths were present), indicating small crystallite size. Representative powder diffraction patterns for selected chromium–iron titanate shear structure compounds and intergrowth phases are given in Fig. 2.

Selected patterns were also fitted using the Rietveld profile refinement method to confirm phase identification. Structures were available for Fe_2O_3 and Cr_2O_3, orthorhombic M_3O_5 (pseudobrookite), and the monoclinic phases M_3O_5, M_4O_7, and M_5O_9.

Electron microprobe studies. Part of each pellet was mounted in epoxy resin, polished, and analyzed for Cr, Fe, and Ti using a JEOL 8900R Superprobe operating in the wavelength dispersive (WDS) mode. Hematite (Fe_2O_3), rutile, and chromium oxide were employed as standards. Points for analysis were selected using high-quality backscattered electron imaging. An accelerating voltage of 15 kV, a sample current of 25 nA, and a beam diameter of 1–3 μm were standard operating conditions. Counting times for Fe, Ti, and Cr were 40 s on the peak and 10 s on each side of the background; 15–20 spot analyses were measured on each phase and their mean composition was calculated.

Experiments conducted at the 1200°C isotherm produced a grain size which was noticeably coarser than that observed

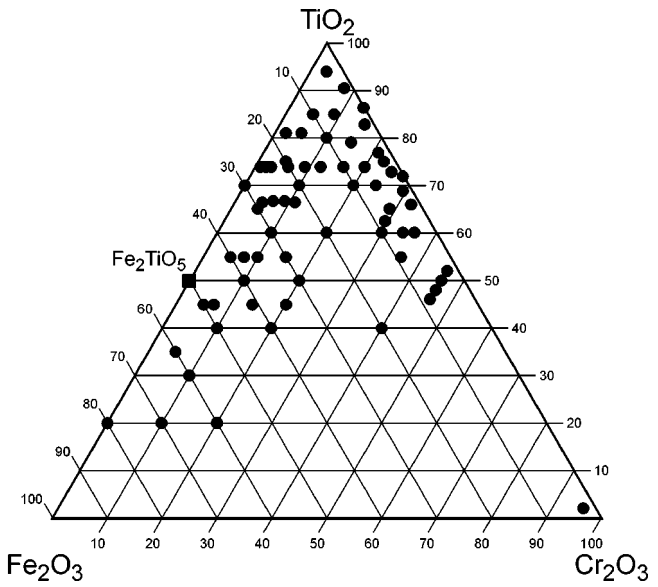

FIG. 1. Compositions, mol%, of starting mixtures in the system Fe_2O_3–Cr_2O_3–TiO_2. Actual compositions reported in Table 1.

in the lower temperature experiments. Consequently, the most complete EMP data set was obtained from the 1200°C series of experiments. In addition to the temperature effect on grain size, we also observed a considerable influence arising from the bulk composition. For example, compositions near to or along the Cr_2O_3–TiO_2 binary join (e.g., compositions 35–37 and also compositions from about 43 to 59) invariably produced fine-grained assemblages, generally $\leq$ 2–3 μm in diameter. This grain size is close to, or slightly smaller than, the excitation volume of the EMP beam, meaning that it was difficult to obtain reliable EMP analytical data from these compositions, even at 1200°C. In comparison, Fe_2O_3-rich compositions produced grain sizes averaging 20–30 μm in diameter. This relatively coarse grain size was also present in the high-Fe_2O_3 bulk compositions annealed at 1100 and 1000°C, enabling EMP data to be obtained for most of these charges.

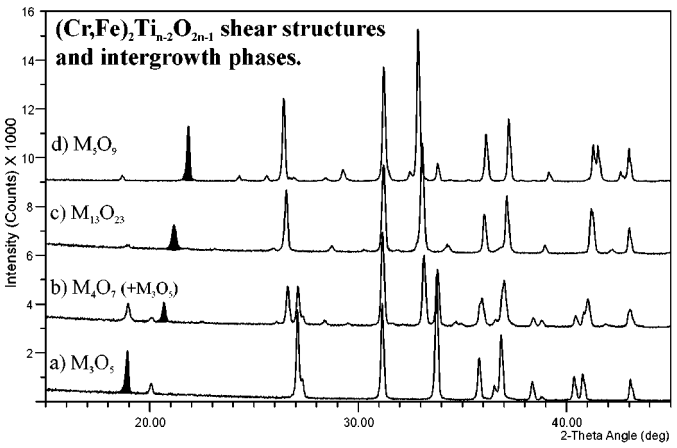

FIG. 2. Representative powder diffraction patterns for selected chromium–iron titanate shear structure compounds and intergrowth phases. All patterns shown are from experiments conducted at 1200°C. Phases were identified using the change in position of the peak between approximately 18.9° and 22° 2θ (shaded).

RESULTS AND DISCUSSION

Results of phase equilibria studies in the system Fe_2O_3–Cr_2O_3–TiO_2 at 1200, 1100, and 1000°C are given in Table 2 and presented schematically in Figs. 3a–3c. The positions of the phase boundaries have been constructed using the observed equilibrium assemblages (from PXRD) and, where possible, the measured compositions of coexisting phases as determined by electron microprobe.

The Fe_2O_3–Cr_2O_3–TiO_2 ternary comprises five major solid solution series. These are as follows: an M_2O_3 series based upon complete solid solution between end members Cr_2O_3 and Fe_2O_3 (and incorporating some TiO_2); an M_3O_5 series made up of two separate solid solution series—the first an orthorhombic pseudobrookite M_3O_5 solid solution and the second an M_3O_5 series based on the monoclinic V_3O_5 structure; an M_4O_7 series; and an M_5O_9 series. These latter three series represent the lower homologues ($n = 3$, 4, and 5) of the $Cr_2Ti_{n-2}O_{2n-1}$ phase series which are stabilized in the ternary via the presence of Fe^{3+}.

In addition to these five solid solution series, there are phase stability regions between adjacent M_3O_5 and M_4O_7 and M_4O_7 and M_5O_9 solid solutions which may contain ordered intergrowths, an Andersson phase series along the Cr_2O_3–TiO_2 binary join, a high-TiO_2, continuous *CS* structure series which extends well into the ternary (denoted as "$Cont_{(CS)}$"), and a rutile-based solid solution. Where possible, compositional limits for the individual solution series are listed in Table 3 while a detailed analysis of the different solid solution series and phase regions are considered separately below.

M_2O_3 Solid Solution Series

At 1200°C, there is complete solid solution between Fe_2O_3 and Cr_2O_3, in agreement with the data of Muan and Sōmiya (1). However, in addition to solid solution along the binary, EMP data also indicate a substantial solubility of TiO_2 in the M_2O_3 solution (see Fig. 3a). For example, bulk composition 1, which equilibrates within the M_2O_3 + Psb two-phase field, has an M_2O_3 phase that contains 11.9 mol% TiO_2. At higher Cr_2O_3 contents (e.g., bulk composition 13), the solubility of TiO_2 in the M_2O_3 solid solution initially decreases to $\sim$ 8–9 mol% before increasing again to $\sim$ 15 mol% (compositions 36 and 37). There is an invariant point along the Fe_2O_3–Cr_2O_3 pseudobinary located at approximately 13.3% TiO_2, 22.0% Cr_2O_3, 64.7%

TABLE 2
Summary of Results for Phase Equilibrium Experiments in the System Fe_2O_3–Cr_2O_3–TiO_2; Phases Listed in Approximate Order of Abundance; Phases in Bold Are Believed To Be Metastable (See Text for Details)

Sample no.	Phase assemblage		
	1200	1100	1000
1	M_2O_3 + Psb	M_2O_3 + Psb	M_2O_3 + Psb
2	M_2O_3 + Psb + M_3O_5(t)	M_2O_3 + M_3O_5	M_2O_3 + M_3O_5
3	M_2O_3 + Psb	M_2O_3 + Psb	M_2O_3 + Psb
4	M_2O_3 + Psb	M_2O_3 + Psb	M_2O_3 + Psb
5	Psb + M_2O_3	Psb + M_2O_3 + M_3O_5	M_2O_3 + Psb + M_3O_5
6	Psb + M_2O_3	Psb + M_2O_3	Psb + M_2O_3
7	M_3O_5 + M_2O_3	M_3O_5 + M_2O_3	M_3O_5 + M_2O_3
8	Psb + M_3O_5 + M_2O_3(t)	Psb + M_3O_5 + M_2O_3(t)	M_3O_5 + Psb + M_2O_3(t)
9	Psb + M_4–M_5 ($M_{13}O_{23}$)	Psb + M_5O_9 + M_3O_5(t)	Psb + M_5O_9 + M_3O_5(t)
10	M_3O_5	M_3O_5	M_3O_5 + M_5O_9(t)
11	M_4O_7 + Psb + M_3O_5	M_3O_5 + M_4–M_5 + Psb	M_3O_5 + M_5O_9
12	Psb + M_5O_9	Psb + M_5O_9	Psb + M_5O_9 + Cont + ***M_2O_3*(t)**
13	M_3O_5 + M_2O_3	M_3O_5 + M_2O_3	M_3O_5 + M_2O_3
14	M_3O_5 + M_4O_7	M_3O_5 + M_5O_9 + **M_4–M_5(t)**	M_3O_5 + M_5O_9
15	M_4–M_5($M_{13}O_{23}$) + M_4O_7(t)	M_5O_9 + M_3O_5 + ***M_4–M_5*(t)**	M_5O_9 + M_3O_5 + **Cont(t)**
16	M_5O_9 + Psb + Cont(t)	M_5O_9 + Psb + Cont(t)	M_5O_9 + Psb + Cont(t)
17	M_3O_5 + M_4O_7	M_5O_9 + M_3O_5 + ***M_4–M_5*(t)**	M_5O_9 + M_3O_5 + M_2O_3
18	M_4–M_5 ($M_{13}O_{23}$)	M_5O_9 + M_3O_5(t)	M_5O_9 + M_3O_5 + **Cont(t)**
19	M_5O_9 + Cont	M_5O_9 + Cont(t)	M_5O_9 + Cont(t) + ***M_3O_5*(t)**
20	M_5O_9 + Cont	M_5O_9 + Cont(t)	M_5O_9 + Cont(t) + ***M_3O_5*(t)**
21	M_5O_9 + Cont	M_5O_9 + Cont	M_5O_9 + Cont(t) + Psb(t) + ***M_3O_5*(t)**
22	Psb + Cont + M_5O_9(t)	Psb + M_5O_9 + Cont	Psb + M_5O_9 + Cont + ***M_2O_3*(t)**
23	M_5O_9 + Psb	M_5O_9 + Psb	M_5O_9 + M_3O_5(t) + Psb(t)
24	M_5O_9 + M_4–M_5(t)	M_5O_9 + M_3O_5(t)	M_5O_9 + M_3O_5 + **Cont(t)**
25	M_5O_9 + M_4–M_5(t)	M_5O_9 + M_3O_5(t)	M_5O_9 + M_3O_5 + **Cont(t)**
26	M_5O_9 + M_4–M_5(t)	M_5O_9 + M_3O_5(t)	M_5O_9 + M_3O_5 + **Cont(t)**
27	Psb + M_2O_3	Psb + M_2O_3 + M_3O_5	Psb + M_2O_3 + M_3O_5
28	Psb + M_3O_5 + M_2O_3	M_3O_5 + M_2O_3	M_3O_5 + M_2O_3
29	M_3O_5 + M_2O_3	M_3O_5 + M_2O_3	M_3O_5 + M_2O_3
30	Psb + M_3O_5 + M_4O_7	Psb + M_3O_5 + M_4O_7	Psb + M_3O_5 + M_5O_9 + ***M_2O_3*(t)**
31	Psb + M_3O_5 + M_4O_7	M_3O_5 + Psb + M_4O_7	M_3O_5 + M_5O_9
32	M_3O_5 + M_4O_7	M_3O_5 + M_5O_9 + ***M_4–M_5*(t)**	M_3O_5 + M_5O_9
33	M_5O_9 + Cont	M_5O_9 + Cont	M_5O_9 + Cont + ***M_3O_5*(t)**
34	M_5O_9 + Cont	M_5O_9 + Cont	M_5O_9 + Cont + ***M_3O_5*(t)**
35	M_2O_3 + M_5O_9	M_2O_3 + Cont + M_5O_9	M_2O_3 + Cont
36	M_4O_7 + M_2O_3	M_2O_3 + M_3O_5 + M_5O_9(t)	M_2O_3 + Cont + M_5O_9
37	M_3O_5 + M_3–M_4 ($M_{11}O_{19}$) + M_2O_3	M_2O_3 + M_3O_5 + M_5O_9(t)	M_2O_3 + M_5O_9 + Cont
38	M_5O_9 + M_4–M_5(t)	M_5O_9 + M_3O_5(t)	M_5O_9 + M_3O_5(t) + **Cont(t)**
39	M_4O_7 + M_3O_5(t)	M_5O_9 + M_3O_5 + ***M_4–M_5*(t)**	M_5O_9 + M_3O_5 + **Cont(t)**
40	Psb + M_5O_9	Psb + M_5O_9	Psb + M_5O_9 + Cont(t) + ***M_2O_3*(t)**
41	M_4–M_5 ($M_{13}O_{23}$) + Psb	M_5O_9 + Psb + ***M_4O_7*(t)** + **M_4–M_5(t)**	M_5O_9 + M_3O_5 + Psb
42	M_4O_7 + M_3O_5(t) + Psb(t)	M_4O_7 + M_3O_5(t)	M_5O_9 + M_3O_5
43	M_5O_9	M_5O_9	M_5O_9 + M_2O_3 + Cont
44	M_3–M_4 ($M_{11}O_{19}$) + M_3O_5	***M_4O_7*** + M_2O_3 + M_3O_5 + ***M_4–M_5*(t)**	M_5O_9 + M_2O_3
45	M_4O_7 + M_2O_3	M_5O_9 + M_2O_3	M_5O_9 + M_2O_3 + Cont(t)
46	M_3O_5 + M_2O_3	M_2O_3 + M_3O_5 + M_4O_7	M_2O_3 + M_5O_9 + M_3O_5(t)
47	M_4–M_5 ($M_{13}O_{23}$)	M_5O_9 + ***M_4O_7*** + **M_4–M_5(t)**	M_5O_9 + M_2O_3 + M_3O_5(t)
48	M_3–M_4 ($M_{11}O_{19}$) + M_3O_5	***M_4O_7*** + M_3O_5 + **M_4–M_5(t)** + M_5O_9(t)	M_5O_9 + M_3O_5 + M_2O_3
49	Cont + M_5O_9(t)	n.d.	n.d.
50	$Cr_2Ti_7O_{17}$ + $Cr_2Ti_6O_{15}$	Cont + M_2O_3 + ***M_5O_9*(t)** + ***M_4–M_5*(t)**	n.d.
51	$Cr_2Ti_3O_9$ + M_2O_3 + $Cr_2Ti_6O_{15}$	M_2O_3 + Cont + ***M_5O_9*(t)** + ***M_4–M_5*(t)**	n.d.
52	M_5O_9 + AP($Cr_2Ti_7O_{17}$ + $Cr_2Ti_6O_{15}$)	M_5O_9 + Cont	n.d.
53	M_2O_3	M_2O_3	n.d.
54	M_5O_9 + Cont	M_5O_9 + Cont	n.d.
55	M_4O_7 + M_3O_5	***M_4O_7*** + M_3O_5 + M_5O_9(t) + ***M_4–M_5*(t)**	n.d.

TABLE 2—*Continued*

Sample no.	Phase assemblage		
	1200	1100	1000
56	$M_3O_5 + M_4O_7$	$M_3O_5 + \boldsymbol{M_4O_7} + M_5O_9$(t)	n.d.
57	$M_5O_9 + M_4$–M_5	n.d.	n.d.
58	$M_5O_9 + M_2O_3 + M_4$–M_5(t)	n.d.	n.d.
59	$M_5O_9 + M_2O_3 + M_4$–M_5(t)	n.d.	n.d.
60	Cont	Cont	n.d.
61	Psb + Cont + TiO_2(??)	Psb + Cont + TiO_2(t)	n.d.
62	Psb + Cont	Psb + Cont	n.d.
63	Psb + Cont	Psb + Cont	n.d.
64	Psb + TiO_2	Psb + TiO_2	n.d.
65	M_2O_3 + Psb	M_2O_3 + Psb	n.d.

Note. Key to abbreviations used: $M_2O_3 = (Fe,Cr)_2O_3$ solid solution; Psb = Pseudobrookite solid solution; M_3O_5 = monoclinic $(Fe,Cr)_2TiO_5$ solid solution; M_4O_7 = monoclinic $(Fe,Cr)_2Ti_2O_7$ solid solution; M_5O_9 = monoclinic $(Fe,Cr)_2Ti_3O_9$ solid solution; M_4–M_5 = M_4O_7–M_5O_9 intergrowth phase; M_3–M_4 = M_3O_5–M_4O_7 intergrowth phase; AP = Andersson phase; Cont = Continuous crystallographic shear structure series; n.d. = not determined.

Fe_2O_3. This point represents the intersection of tie lines that separate the phase fields Psb + M_2O_3, Psb + M_2O_3 + M_3O_5, and $M_2O_3 + M_3O_5$ (Fig. 3a).

The M_2O_3 solid solution phase field intersects the Fe_2O_3–TiO_2 binary at 12.3 mol% TiO_2. MacChesney and Muan (2) examined phase relations along the Fe_2O_3–(Fe_3O_4)–TiO_2 pseudobinary at $T \geq 1400$°C, and extrapolation of their data to 1200°C indicates a solubility of TiO_2 in Fe_2O_3 of approximately 12–13 mol%, in excellent agreement with the results from this study. For the Cr_2O_3–TiO_2 binary, Yakshibaev and Gaitova (20) examined solid solution formation in high-Cr_2O_3, low-TiO_2 mixtures by measuring the thermal expansion coefficient of chromium oxide doped with TiO_2 between 400 and 1000°C. They found that a maximum of $\sim$ 15 wt% TiO_2 (25 mol%) could be incorporated into Cr_2O_3. For comparison, EMP data for the M_2O_3 phase formed by annealing composition 51 at 1200°C gives a solubility of TiO_2 in Cr_2O_3 of 23 mol%. This result is in good agreement with the Yakshibaev and Gaitova (20) data (although our solubility value has an associated 1σ error of at least $\pm$ 2–3 mol% TiO_2 resulting from the fine grain size of the annealed sample).

Lowering the temperature of annealing to below 1200°C results in a systematic decrease in the extent of TiO_2 incorporation into the Fe_2O_3–Cr_2O_3 solution series (Figs. 3b and 3c). Along the Fe_2O_3–TiO_2 binary, the solubility of TiO_2 in Fe_2O_3 decreases to 8.4 mol% at 1100°C and to approximately 5 mol% at 1000°C (extrapolated). The fine grain size of the annealed samples prevented the determination of TiO_2 solubility results for the Cr_2O_3–TiO_2 binary at $T < 1200$°C. The dashed phase boundaries shown in Figs. 3b and 3c are an approximation only based on the low-temperature data of Yakshibaev and Gaitova (20). For both these low-temperature isotherms there is also a systematic change in the location of the invariant point that separates the Psb + M_2O_3, Psb + M_2O_3 + M_3O_5, and M_2O_3 + M_3O_5 phase fields. The invariant point shifts from approximately 8.1% TiO_2, 21.9% Cr_2O_3, 70.0% Fe_2O_3 to 6.2% TiO_2, 18.6% Cr_2O_3, 75.2% Fe_2O_3 at 1100 and 1000°C, respectively (values quoted in mol%).

M_3O_5 Solid Solution Series

There are two separate $(Cr,Fe)_2Ti_{n-2}O_{2n-1}$ (where $n = 3$) solid solution series. The first M_3O_5 series has the pseudobrookite (Psb) structure and, according to Kwestroo and Roos (16) and Grey and Reid (17), up to $\sim$ 15 mol% of Fe_2O_3 can be replaced by Cr_2O_3 without change of structure (at temperatures between 1250 and 1300°C). For comparison, EMP results from this study show that, at 1200°C, up to 12 mol% Cr_2O_3 may be incorporated into the pseudobrookite structure. At higher Cr_2O_3 contents, the pseudobrookite structure decomposes and there exists a two-phase region comprising pseudobrookite and a second M_3O_5 phase that is isomorphous with the V_3O_5 structural type (16). Quantitative EMP results from composition 8 where both M_3O_5 structure types coexist indicate that the two-phase region extends from approximately 12 mol% to 29 mol% Cr_2O_3 at 1200°C. Beyond 29 mol% Cr_2O_3, a monoclinic V_3O_5 structure-type solid solution series becomes stable. Formation of the V_3O_5 solution series is dependent on the Cr:Fe ratio with the solid solution being restricted to the compositional range of 29–86 mol% Cr_2O_3. Beyond 86 mol% Cr_2O_3, the V_3O_5 structure is no longer stable and decomposes to produce a three-phase region comprising the assemblage $M_3O_5 + M_4O_7 + M_2O_3$ (Fig. 3a).

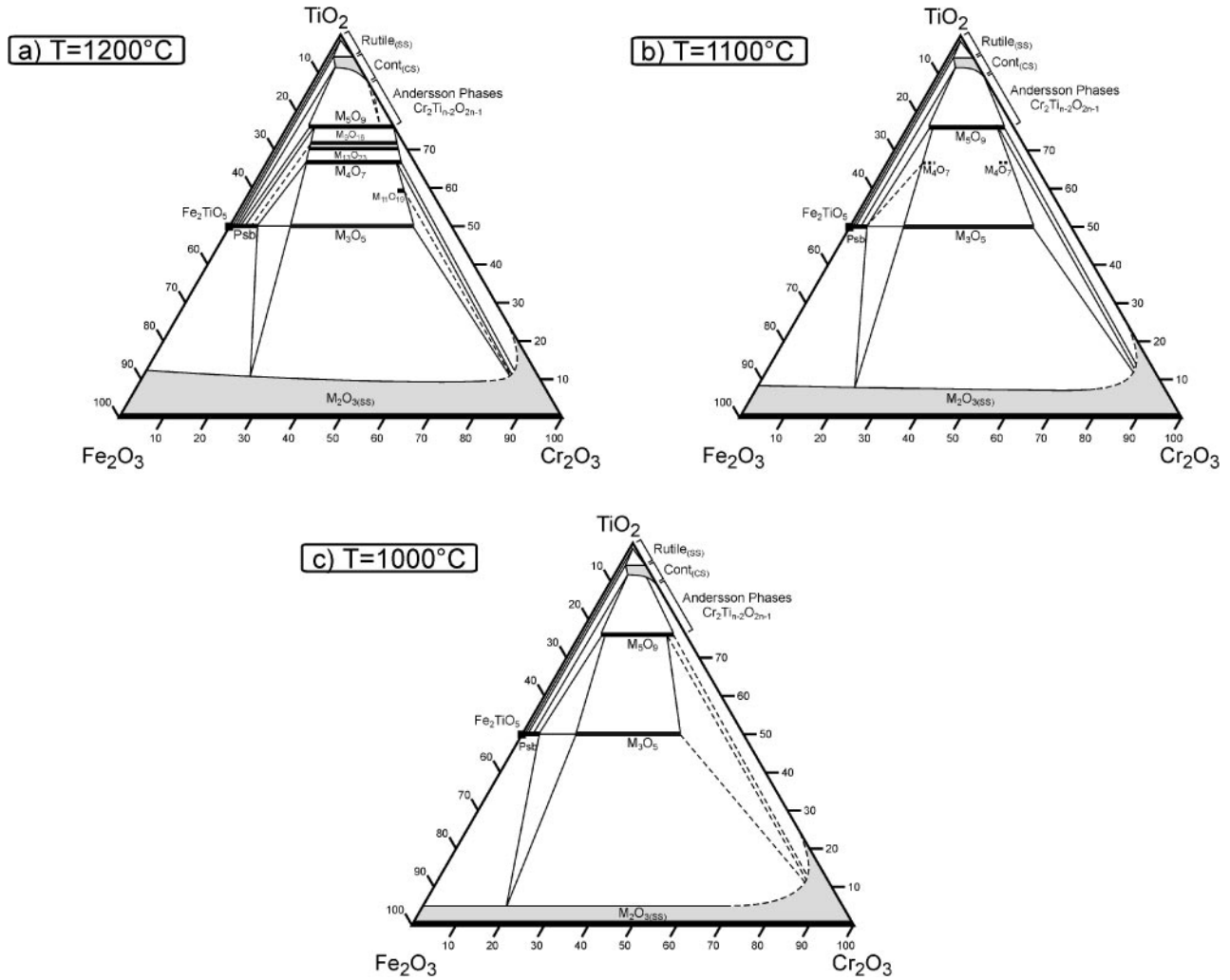

FIG. 3. Phase relations in the system Fe_2O_3–Cr_2O_3–TiO_2 in air at (a) 1200°C, (b) 1100°C, and (c) 1000°C. In each diagram, solid lines indicate the presence of a solid solution series, shaded areas are regions of Cr:Fe:Ti mutual solubility, light lines represent boundaries between phase regions, and dashed lines indicate uncertain phase boundaries.

Lowering the equilibration temperature to 1100°C has only a slight impact upon the extent of solid solution within both M_3O_5 series (Fig. 3b). Based on EMP data, the maximum extent of Cr_2O_3 incorporation into Psb decreases marginally to around 9–10 mol% Cr_2O_3 at 1100°C, while the V_3O_5 structure-type solid solution series ranges from 25 to 84 mol% Cr_2O_3.

A further decrease in temperature to 1000°C results in the V_3O_5 structure-type solid solution series being restricted to between 22 and 80 mol% Cr_2O_3 (Fig. 3c). At 1000°C, the Psb composition can contain up to ~ 7 mol% Cr_2O_3 before decomposing to the Psb + M_3O_5 two-phase assemblage.

M_4O_7 Solid Solution Series

At 1200°C, the pure chromium end member of the $(Cr,Fe)_2Ti_{n-2}O_{2n-1}$ (where $n = 4$) series, $Cr_2Ti_2O_7$, was not stable. Within the ternary, however, replacement of Cr_2O_3 by Fe_2O_3 results in the formation of single-phase M_4O_7 with the solid solution series extending from ~ 92 to 29 mol% Cr_2O_3. The low-Cr_2O_3 member of the solid solution series is well constrained via quantitative EMP analysis whereas the upper Cr_2O_3 limit for M_4O_7 is less certain due to the fine-grained nature of the phase precluding accurate EMP analysis. At Cr_2O_3 contents less than 29 mol%, single-phase M_4O_7 breaks down to the two-phase assemblage M_3O_5(Psb structure) + M_4–M_5 (where M_4–M_5 represents an ordered intergrowth between adjacent M_4O_7 and M_5O_9 homologues).

At 1100°C, the M_4O_7 series is unstable relative to the two-phase assemblage $M_3O_5 + M_5O_9$. Note that some bulk compositions, particularly at high-Cr_2O_3 contents (e.g., compositions 44, 47, 48, 55, and 56), have minor amounts of M_4O_7 as part of the phase assemblage (Table 2). These compositions, however, also comprise either M_3O_5 (V_3O_5 structure type), M_5O_9, or an M_4–M_5 intergrowth, in

TABLE 3
Summary of EMP Composition Data for Solid Solution Series and Intergrowth Phases within the Fe_2O_3–Cr_2O_3–TiO_2 system

Solution series	Temp. (°C)	Composition range
M_2O_3	1000	Continuous between 5 mol% TiO_2 in Fe_2O_3 (*approx.*) and 23–25 mol% TiO_2 in Cr_2O_3 (*approx.*)
	1100	Continuous between 8.4 mol% TiO_2 in Fe_2O_3 and 23–25 mol% TiO_2 in Cr_2O_3 (*approx.*)
	1200	Continuous between 12.3 mol% TiO_2 in Fe_2O_3 and 23–25 mol% TiO_2 in Cr_2O_3 (*approx.*)
	1300	Continuous between 16.3 mol% TiO_2 in Fe_2O_3 and 23–25 mol% TiO_2 in Cr_2O_3 (*approx.*)
M_3O_5	1000	Psb: $Fe_2TiO_5 \rightarrow (Fe_{0.93}Cr_{0.07})_2TiO_5$
		V_3O_5: $(Fe_{0.78}Cr_{0.22})_2TiO_5 \rightarrow (Fe_{0.20}Cr_{0.80})_2TiO_5$
	1100	Psb: $Fe_2TiO_5 \rightarrow (Fe_{0.91}Cr_{0.09})_2TiO_5$
		V_3O_5: $(Fe_{0.75}Cr_{0.25})_2TiO_5 \rightarrow (Fe_{0.16}Cr_{0.84})_2TiO_5$
	1200	Psb: $Fe_2TiO_5 \rightarrow (Fe_{0.88}Cr_{0.12})_2TiO_5$
		V_3O_5: $(Fe_{0.71}Cr_{0.29})_2TiO_5 \rightarrow (Fe_{0.14}Cr_{0.86})_2TiO_5$
	1300	Psb: $Fe_2TiO_5 \rightarrow$ $(Fe_{0.84}Cr_{0.16})_2TiO_5$ (*approx.*)
		V_3O_5: $(Fe_{0.68}Cr_{0.32})_2TiO_5$ (*approx.*) $\rightarrow (Fe_{0.10}Cr_{0.90})_2TiO_5$ (*approx.*)
M_4O_7	1000	Not stable
	1100	Not stable
	1200	$(Fe_{0.71}Cr_{0.29})_2Ti_2O_7 \rightarrow (Fe_{0.08}Cr_{0.92})_2Ti_2O_7$ (*approx.*)
	1300	$(Fe_{0.71}Cr_{0.29})_2Ti_2O_7$(*approx.*) $\rightarrow (Fe_{0.09}Cr_{0.91})_2Ti_2O_7$ (*approx.*)
M_5O_9	1000	$(Fe_{0.77}Cr_{0.23})_2Ti_3O_9 \rightarrow (Fe_{0.15}Cr_{0.85})_2Ti_3O_9$
	1100	$(Fe_{0.77}Cr_{0.23})_2Ti_3O_9 \rightarrow (Fe_{0.07}Cr_{0.93})_2Ti_3O_9$
	1200	$(Fe_{0.77}Cr_{0.23})_2Ti_3O_9 \rightarrow Cr_2Ti_3O_9$
	1300	$(Fe_{0.73}Cr_{0.27})_2Ti_3O_9$ (*approx.*) $\rightarrow Cr_2Ti_3O_9$
$M_{11}O_{19}$ (M_3–M_4)	1200	$(Fe_{0.15}Cr_{0.85})_6Ti_5O_{19} \rightarrow (Fe_{0.12}Cr_{0.88})_6Ti_5O_{19}$ (*approx.*)
M_9O_{16} (M_4–M_5)	1200	$(Fe_{0.75}Cr_{0.25})_2Ti_7O_{16}$ (*approx.*) $\rightarrow (Fe_{0.05}Cr_{0.95})_2Ti_7O_{16}$ (*approx.*)
$M_{13}O_{23}$ (M_4–M_5)	1200	$(Fe_{0.74}Cr_{0.26})_2Ti_{11}O_{23} \rightarrow (Fe_{0.66}Cr_{0.34})_2Ti_{11}O_{23}$ (*approx.*)

phase combinations which suggest that M_4O_7 is probably metastable in this region of the ternary system. In contrast, at high-Fe_2O_3 bulk compositions (e.g., compositions 30, 31, and 42), there appears to be a localized region where a limited M_4O_7 solid solution series may be stabilized.

M_4O_7 phase was not detected in any compositions equilibrated at 1000°C.

M_5O_9 Solid Solution Series

At 1200°C, the $(Cr,Fe)_2Ti_{n-2}O_{2n-1}$ (where $n = 5$) solid solution series extends from at or close to pure $Cr_2Ti_3O_9$, to a composition containing 23 mol% Cr_2O_3 (EMP data for composition 16). Lowering the annealing temperature to 1100 and 1000°C causes the high-Cr_2O_3 end of the M_5O_9 solution series to contract to approximately 93 and 85 mol% Cr_2O_3, respectively. The low-Cr_2O_3 limit of the M_5O_9 solution remains fixed at around 23 mol% Cr_2O_3 for both isotherms.

Note that, for compositions annealed at 1000°C where M_5O_9 was present in the final assemblage, the run products were nearly always contaminated by an additional phase. The composition of the extra phase was dependent on the bulk composition of the starting mixture, with charges annealed in the M_5O_9 + AP field containing trace amounts of M_3O_5 phase, whereas charges *lower* in TiO_2, which equilibrated in the $M_5O_9 + M_3O_5$ phase field, contained trace quantities of AP. Similar observations were also reported by Grey and Reid (17) who concluded, that in addition to a delicate balance between Fe:Cr content (with M_5O_9 phase favored, by high Fe contents), there is only a narrow temperature range over which single-phase M_5O_9 can be obtained. It is unclear in the current study, however, whether these extraneous phases represent the failure of the charges to fully equilibrate (i.e., metastable persistence of intermediate phases) or reflect the rapid, low-temperature breakdown of M_5O_9 upon quenching.

An interesting observation from the 1200°C experiments concerns the stability of the pure end member M_5O_9 phase, $Cr_2Ti_3O_9$. Most previous studies of the Cr_2O_3–TiO_2 binary are limited to temperatures above 1250–1300°C and, besides the work of Sōmiya *et al.* (15), usually do not report the

existence of $Cr_2Ti_3O_9$. Sōmiya *et al.* (15), however, show $Cr_2Ti_3O_9$ as being stable between 1250 and 1300°C, although the low-temperature limit is unknown. Early work by Grey and Reid (17) indicated that $Cr_2Ti_3O_9$ is not stable and Andersson phases (AP) are produced when a composition consisting of $Cr_2O_3 \cdot 3TiO_2$ is annealed at 1200°C. Although a composition representing pure $Cr_2Ti_3O_9$ was not examined in the current study, composition 51 (Table 1), which was prepared along the Cr_2O_3–TiO_2 binary, crystallized the assemblage $Cr_2O_3 + Cr_2Ti_3O_9 + AP$(trace). This assemblage is not thermodynamically possible and indicates that equilibrium was probably not reached. Nonetheless, $Cr_2Ti_3O_9$ was clearly present in the experimental run products, suggesting it can be stable at temperatures as low as 1200°C—but presumably reaction kinetics are extremely sluggish within the Cr_2O_3–TiO_2 system and further firing/grinding of the sample is required. As soon as Fe is added to the reacting system, however (e.g., compositions 57 and 58), M_5O_9 readily forms and Andersson phases cease to exist. The apparent discrepancy with the Grey and Reid (17) result is attributed to the fact that Grey and Reid annealed their sample at 1200°C for only 2 days and may not have attained equilibrium. In contrast, the results of the current study at 1200°C were obtained on a sample annealed for up to 300 h with an intermediate grinding stage to promote equilibrium.

M_3O_5–M_4O_7 Intergrowth Region

At 1200°C, the region of the phase diagram between the M_3O_5 and M_4O_7 solid solution series is mainly characterized by the two-phase assemblage $M_3O_5 + M_4O_7$. However, as the bulk starting compositions become more Cr_2O_3-rich (e.g., toward bulk compositions 44 and 48), an ordered intergrowth phase between M_3O_5 and M_4O_7 is present in the experimental run products. Based on results from PXRD analysis, the structure type of the intergrowth is $M_{11}O_{19}$ ($3M_2O_3 \cdot 5TiO_2$; 62.5% TiO_2).

The $M_{11}O_{19}$ intergrowth always occurs associated with M_3O_5 and there appears to be a restricted chromium:iron:titanium range where it is stabilized. For example, composition 17, which crystallizes only the $M_3O_5 + M_4O_7$ two-phase assemblage, has the same TiO_2 content as composition 44 but a *lower* Cr:Fe ratio. Similarly, compositions 55 and 56, which have Cr:Fe ratios midway between that of compositions 44 and 48 (but differ in TiO_2 content), also only produce the assemblage $M_3O_5 + M_4O_7$. The fact that these latter two compositions show no evidence of $M_{11}O_{19}$ formation suggests that the intergrowth is probably metastable, i.e., if $M_{11}O_{19}$ was a stable phase, it is expected that composition 55 would comprise the assemblage $M_4O_7 + M_{11}O_{19}$ while composition 56 would produce $M_3O_5 + M_{11}O_{19}$. Evidently, if the bulk composition is not within the favorable chromium:iron:titanium range, $M_{11}O_{19}$ does not form. Conversely, if the bulk composition does fall within the range, once the alternating slabs of V_3O_5 and α-PbO_2 structural types initially achieve long-range order to create the $M_{11}O_{19}$ intergrowth, it becomes energetically difficult to re-order the structure back to $M_3O_5 + M_4O_7$.

The $M_{11}O_{19}$ intergrowth phase was not detected in any compositions equilibrated at 1100 or 1000°C.

M_4O_7–M_5O_9 Intergrowth Region

The phase region between M_4O_7 and M_5O_9 is complex at 1200°C due to a number of intergrowth phases being stabilized. Close to M_5O_9 there exists a two-phase region comprising the assemblage $M_5O_9 + M_9O_{16}$ (where $M_9O_{16} = 2M_2O_3 \cdot 5TiO_2$; 71.4% TiO_2). The M_9O_{16} intergrowth phase was very fine-grained, and accurate EMP data was not obtainable. Nonetheless, based on the PXRD results from bulk compositions 24–26, 38, and 57, M_9O_{16} appears to be stable from approximately 95 mol% Cr_2O_3 (close to composition 57) to $\sim$ 25 mol% Cr_2O_3 (i.e., slightly contracted at the low-Cr_2O_3 end relative to the compositional range exhibited by the M_5O_9 solid solution series).

At slightly lower TiO_2 contents, a second intergrowth phase is stable. Compositions 15, 18, and 47 all record the presence of an $M_{13}O_{23}$ phase (where $M_{13}O_{23} = 3M_2O_3 \cdot 7TiO_2$; 70% TiO_2). The bulk starting mixtures for these three compositions all contain 70 mol% TiO_2 and therefore fall along the stoichiometric $M_{13}O_{23}$ plane. Compositions 18 and 47, however, show single-phase $M_{13}O_{23}$ only, while composition 15 contains a trace amount (< 1–2%) of M_4O_7 phase. In contrast to the M_9O_{16} phase, the $M_{13}O_{23}$ material appeared much coarser in grain size. EMP data was obtainable for the low-Cr_2O_3 end of the intergrowth series, giving a composition containing $\sim$ 26 mol% Cr_2O_3. This value is similar to the low-Cr_2O_3 composition estimated above for the M_9O_{16} intergrowth series which lies parallel and suggests that both intergrowth series have a comparable compositional range (see Fig. 3a).

The presence of M_4–M_5 intergrowth phase(s) was not detected in any compositions equilibrated at 1100 or 1000°C.

Rutile, Andersson Phase (AP), and Continuous Crystallographic Shear Structure Series ($Cont_{(CS)}$) Stability Regions

In the $(Cr,Fe)_2Ti_{n-2}O_{2n-1}$ series there were no homologues with $n > 5$, and $n = 5$ appears to correspond to the maximum size of the slabs of the α-PbO_2-type structure, which may be stabilized in this system in air. In support of this, annealed bulk compositions that were richer in TiO_2 than the M_5O_9 ($n = 5$) solid solution series formed three distinct phase regions. At TiO_2 contents greater than about

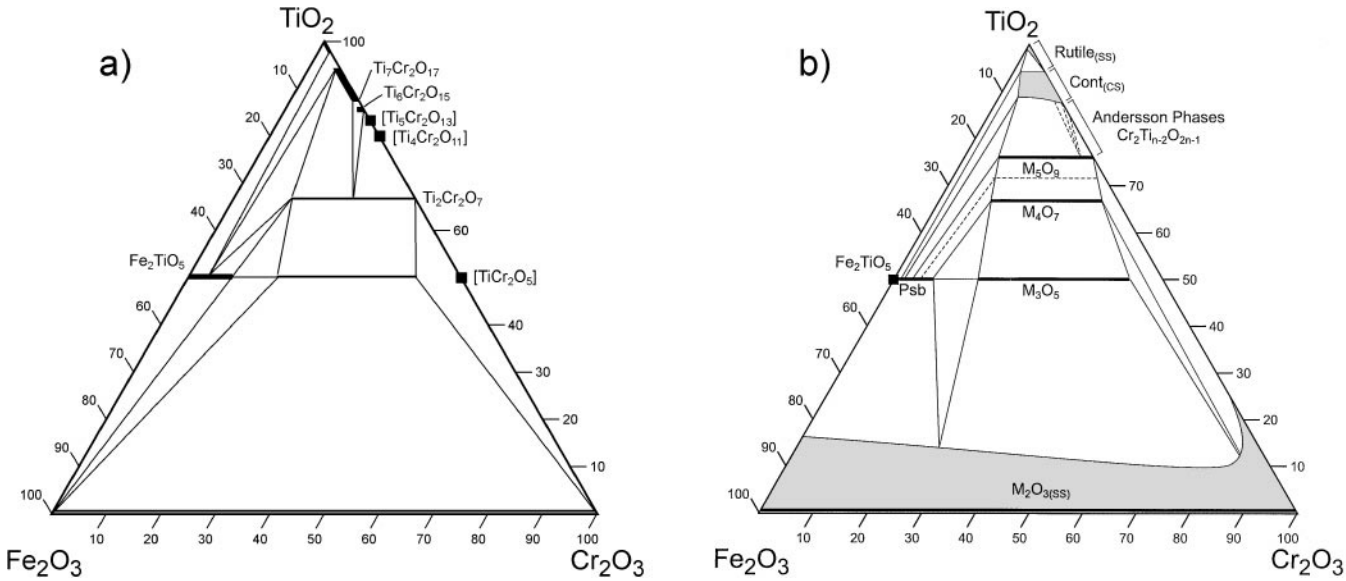

FIG. 4. Comparison of phase relations in the system Fe_2O_3–Cr_2O_3–TiO_2 at 1300°C in air from (a) Kwestroo and Roos (16) and (b) this study. In Fig. 4b, the dashed line between the M_5O_9 and M_4O_7 solution series indicates the possible presence of an M_4–M_5 intergrowth phase (e.g., see composition 38, Table 4).

95 mol%, rutile structure-defect solid solutions were formed. The maximum solubility of Fe_2O_3 in rutile at 1200°C was determined by EMP to be 0.8 mol% (composition 64). Equivalent Cr_2O_3 solubility results along the Cr_2O_3–TiO_2 binary were not measured, however. Previous results from Gibb and Anderson (8) for the high-TiO_2 end of the Cr_2O_3–TiO_2 binary showed that between 1057 and 1297°C, up to 5 mol% Cr_2O_3, may be present in rutile. A systematic study of the extent of this phase region at lower temperatures was not conducted and hence its location, as represented in Figs. 3b and 3c, is approximate only.

Along the Cr_2O_3–TiO_2 binary, at compositions between 5 and 12 mol% Cr_2O_3, a continuous series of well-ordered crystallographic shear phases are formed (8). At 1200°C, the addition of Fe_2O_3 results in extension of these phases into the ternary, producing a phase region denoted as a "continuous crystallographic shear structure series—$Cont_{(CS)}$" (Fig. 3a). EMP data reveal that the continuous *CS* structure series phase field has considerable width (i.e., variation in TiO_2 content) and also extends across the ternary toward higher Fe_2O_3 compositions. The extension to higher Fe_2O_3 compositions proceeds to slightly beyond the limit of the M_5O_9 solid solution series, giving rise to a small three-phase region of Psb + M_5O_9 + $Cont_{(CS)}$ (e.g., composition 22). At more Fe_2O_3-rich compositions, a two-phase Psb + $Cont_{(CS)}$ phase region is encountered (compositions 62 and 63), followed by a narrow three-phase field characterized by the assemblage Psb + $Cont_{(CS)}$ + TiO_2 (composition 61). Beyond this phase region the assemblage Psb + TiO_2 must become stable, although this occurs at very low Cr_2O_3 contents (< 1 mol%), and was not encountered during the present study. The continuous *CS* structure series phase region was also present to a similar extent in the 1100 and 1000°C experiments (Figs. 3b and 3c).

At compositions greater than about 12–13 mol% Cr_2O_3 along the Cr_2O_3–TiO_2 binary, compounds of the known Andersson phase series $Cr_2Ti_{n-2}O_{2n-1}$ can form (8). In compositions with high Cr_2O_3 (e.g., composition 52) the phases $Cr_2Ti_6O_{15}$ ($n = 8$) and/or $Cr_2Ti_7O_{17}$ ($n = 9$) coexisted with M_5O_9 in the 1200°C experiments (Fig. 3a). Trace amounts of Andersson phase products were also identified in the lower temperature experiments. It was not possible to assign a unique composition to any of these phases, however.

Fe_2O_3–Cr_2O_3–TiO_2 System at 1300°C

The only previous study of the Fe_2O_3–Cr_2O_3–TiO_2 system was conducted at 1300°C by Kwestroo and Roos (16)—see Fig. 4a for a reproduction of their results. Although the Kwestroo and Roos (16) study was conducted at a slightly higher temperature than the current results, comparison of Fig. 4a with Figs. 3a–3c indicates significant differences in the interpretation of the phase relations. For example, Kwestroo and Roos (16) did not show the existence of an M_5O_9 solid solution series at 1300°C. This implies that the M_5O_9 solution series that is present at 1000–1200°C must decompose before 1300°C to produce either M_4O_7 + AP (at high-Cr_2O_3 contents) or Psb + M_4O_7 + AP (at low-Cr_2O_3 contents).

As well as a possible temperature effect on M_5O_9 stability, it is significant that Kwestroo and Roos (16) did not

TABLE 4

Summary of 1300°C Experimental Results in the System Fe_2O_3–Cr_2O_3–TiO_2; Phases Listed in Approximate Order of Abundance; Abbreviations Same as in Table 3

Sample no.	Phase assemblage	Sample no.	Phase assemblage
5	Psb + M_2O_3	32	M_3O_5 + M_4O_7
7	M_3O_5 + M_2O_3	38	M_5O_9 + M_4–M_5
9	Psb + M_4–M_5	44	M_3O_5 + M_4O_7
13	M_3O_5 + M_2O_3	45	M_4O_7 + M_2O_3 + M_3O_5
17	M_4O_7 + M_3O_5	46	M_3O_5 + M_2O_3
19	M_5O_9 + Cont	51	M_5O_9 + AP(t) + M_2O_3(?)
21	M_5O_9 + Cont	52	$Cr_2Ti_6O_{15}$ + M_5O_9 + $Cr_2Ti_7O_{17}$(?)
23	Psb + Cont + M_5O_9	61	Psb + Cont
30	Psb + M_3O_5 + M_4O_7(t)	65	M_2O_3 + Psb
31	Psb + M_3O_5 + M_4O_7		

show any evidence of TiO_2 substitution within the Fe_2O_3–Cr_2O_3 solid solution series. In contrast, the 1000–1200°C results from the present study clearly reveal a broad M_2O_3 stability region that extends appreciably into the ternary.

To check on the decomposition of M_5O_9 with temperature and the extent of TiO_2 substitution into M_2O_3, a limited set of compositions was annealed at 1300°C for 48 h. The compositions examined and their resultant assemblages are provided in Table 4 and represented in Fig. 4b. Where possible, compositional limits for the individual solution series were estimated from EMP data and these have been included in Table 3.

Results from the 1300°C series experiments show that the Kwestroo and Roos (16) phase relations for the Fe_2O_3–Cr_2O_3–TiO_2 system are incorrect with the M_5O_9 solid solution series clearly stable at 1300°C, ranging from close to pure $Cr_2Ti_3O_9$ to a composition containing approximately 27 mol% Cr_2O_3. This solid solution range is slightly less than that determined between 1000 and 1200°C, indicating that the high-Fe_2O_3 end of the series may be starting to partially decompose at 1300°C. It is unclear, however, as to why there is a discrepancy with the earlier results, although it is possible that the 3-h annealing time employed by Kwestroo and Roos (16) may have been insufficient to attain equilibrium.

At 1300°C there is significant TiO_2 substitution in the M_2O_3 solution series, in excellent agreement with the current 1000–1200°C data. The M_2O_3 solid solution phase field intersects the Fe_2O_3–TiO_2 binary at 16.3 mol% TiO_2 (EMP data for composition 65) while the equivalent point along the Cr_2O_3–TiO_2 binary was extrapolated to be approximately 25 mol% TiO_2 (see Fig. 4b). The invariant point along the Fe_2O_3–Cr_2O_3 pseudobinary is located at approximately 14.3% TiO_2, 26.6% Cr_2O_3, 59.1% Fe_2O_3.

SUMMARY

Phase equilibria and the stability of crystallographic shear structure compounds $(Cr,Fe)_2Ti_{n-2}O_{2n-1}$ in the system Fe_2O_3–Cr_2O_3–TiO_2 were investigated between 1000 and 1300°C. Quenched samples were examined by powder X-ray diffraction and electron microprobe analytical methods.

The Fe_2O_3–Cr_2O_3–TiO_2 ternary comprises five major solid solution series. These are as follows: an M_2O_3 series based upon complete solid solution between end members Cr_2O_3 and Fe_2O_3 (and incorporating some TiO_2); an M_3O_5 series made up of two separate solid solution series—the first a pseudobrookite M_3O_5 solid solution and the second an M_3O_5 series based on the V_3O_5 structure; an M_4O_7 series; and an M_5O_9 series. These latter three series represent the lower homologues ($n = 3, 4$, and 5) of the $Cr_2Ti_{n-2}O_{2n-1}$ phase series that are stabilized in the ternary via the presence of Fe^{3+}. Note, however, that in the $(Cr,Fe)_2Ti_{n-2}O_{2n-1}$ series there are no homologues with $n > 5$. The stability and compositional limits of each solid solution series is dependent upon the temperature and Fe:Cr ratio.

In addition to these five solid solution series, there are phase stability regions between adjacent M_3O_5–M_4O_7 and M_4O_7–M_5O_9 solid solutions that may contain ordered intergrowths. At 1200°C, an $M_{11}O_{19}$ intergrowth is stabilized within a restricted Cr:Fe:Ti composition region between M_3O_5 and M_4O_7. The $M_{11}O_{19}$ intergrowth phase was not present in any compositions equilibrated at 1100 or 1000°C. Between the M_4O_7 and M_5O_9 solid solution series, two intergrowth phases were present at 1200°C. These comprised an M_9O_{16} and an $M_{13}O_{23}$ series, both of which had comparable compositional ranges. The presence of these two intergrowth phases was not detected in any compositions equilibrated at 1100 or 1000°C.

At high-TiO_2 contents (greater than M_5O_9 or 75% TiO_2), phase relations in the Fe_2O_3–Cr_2O_3–TiO_2 system may be characterized by either an Andersson phase series along the Cr_2O_3–TiO_2 binary join, a high-TiO_2, continuous *CS* structure series that extends significantly into the ternary, or a rutile-based solid solution. The presence (or absence) of any of these phases is composition dependent.

A comparison of the results from the 1300°C series experiments with previously established phase relations for the Fe_2O_3–Cr_2O_3–TiO_2 system (16) shows considerable discrepancy. Results from the 1300°C series experiments show that the Kwestroo and Roos (16) phase relations for the Fe_2O_3–Cr_2O_3–TiO_2 system are incorrect with the M_5O_9 solid solution series clearly stable at 1300°C, ranging from close to pure $Cr_2Ti_3O_9$ to a composition containing approximately 27 mol% Cr_2O_3.

ACKNOWLEDGMENTS

The authors express their gratitude to Tim Patrick (preparation of figures), Cameron Davidson (sample preparation), Nick Wilson and Colin MacRae (microprobe setup), and Dr. Graham Sparrow (manuscript review). Dr. Ian Grey is especially thanked for helpful discussions and historical perspectives regarding previous work in parts of the Fe_2O_3–Cr_2O_3–TiO_2 system as well as a thoughtful review of the final manuscript.

REFERENCES

1. A. Muan and S. Sōmiya, *J. Am. Ceram. Soc.* **42,** 603–613 (1959).
2. J. B. MacChesney and A. Muan, *Am. Mineral.* **44,** 586–591 (1959).
3. R. W. Taylor, *J. Am. Ceram. Soc.* **46,** 276–279 (1963).
4. R. W. Taylor, *Am. Mineral.* **49,** 1016–1030 (1964).
5. D. H. Lindsley, *Carnegie Inst. Wash. Year Book* **64,** 144–148 (1965).
6. I. E. Grey, C. Li, and J. A. Watts, *Am. Mineral.* **68,** 981–988 (1983).
7. L. A. Bursill, B. G. Hyde, and D. K. Philp, *Philos. Mag.* **23,** 1501–1513 (1971).
8. R. M. Gibb and J. S. Anderson, *J. Solid State Chem.* **4,** 379–390 (1972).
9. S. Andersson, A. Sundholm, and A. Magneli, *Acta Chem. Scand.* **13,** 989–997 (1959).
10. S. Andersson, B. Collen, U. Kuylenstierna, and A. Magneli, *Acta Chem. Scand.* **11,** 1641 (1957).
11. G. Andersson, *Acta Chem. Scand.* **8,** 1599 (1954).
12. A. Åsbrink, S. Friberg, A. Magneli, and G. Andersson, *Acta Chem. Scan.* **13,** 604 (1959).
13. M. Hamélin, *Bull. Soc. Chim. Fr.* 1421–1431 (1957).
14. O. W. Flörke and C.W. Lee, *J. Solid State Chem.* **1,** 445–453 (1970).
15. S. Sōmiya, M. Yoshimura, S. Kamiya, and S. Itoh, *Sci. Ceram.* **10,** 257–266 (1980).
16. W. Kwestroo and A. Roos, *J. Inorg. Nucl. Chem.* **13,** 325–326 (1960).
17. I. E. Grey and A. F. Reid, *J. Solid State Chem.* **4,** 186–194 (1972).
18. I. E. Grey and W. G. Mumme, *J. Solid State Chem.* **5,** 168–173 (1972).
19. I. E. Grey, A. F. Reid, and J. G. Allpress, *J. Solid State Chem.* **8,** 86–99 (1973).
20. R. A. Yakshibaev and A. F. Gaitova, *Inorg. Mater.* **21,** 281–282 (1985).